Electronic Supplementary Material (ESI) for Sustainable Energy & Fuels.

Dual vanadium substitution strategy for improving NASICON-type cathode materials in Na-ion batteries

P. Lavela, R. Klee, J.L. Tirado

Departamento de Química Inorgánica e Ingeniería Química. Instituto Universitario de Química Fina y Nanoquímica. Universidad de Córdoba.

Edificio Marie Curie. Campus de Rabanales 14071 Córdoba (Spain)

Table S1. Parameters of the gaussian-lorentzian components calculated from the deconvoluted Raman spectra ascribable to the amorphous carbon phase existing in the $Na_3VCr_{1-x}Al_x(PO_4)_3$ ($0 \leq x \leq 1$) samples.

		D4	D1	D3	G	D2
x= 0.0	Shift/ cm^{-1}	1208.8	1339.2	1502.2	1597.3	1687.9
I_G/I_{D1}=0.471	FWHM /cm^{-1}	129.9	147.1	187.3	80.84	42.2
x= 0.2	Shift/ cm^{-1}	1194.1	1351.6	1502.4	1593.2	1688.0
I_G/I_{D1}=0.472	FWHM /cm^{-1}	175.4	179.6	125.6	93.1	100.9
x= 0.4	Shift/ cm^{-1}	1196.5	1339.8	1496.3	1590.6	1687.3
I_G/I_{D1}=0.466	FWHM /cm^{-1}	187.7	172.3	177.5	90.1	91.5
x= 0.6	Shift/ cm^{-1}	1197.2	1350.1	1502.4	1593.6	1688.0
I_G/I_{D1}=0.471	FWHM /cm^{-1}	191.1	172.9	141.3	93.8	122.1
x= 0.8	Shift/ cm^{-1}	1197.8	1341.7	1499.3	1593.0	1687.3
I_G/I_{D1}=0.462	FWHM /cm^{-1}	160.9	159.2	156.9	88.3	53.49
x= 1.0	Shift/ cm^{-1}	1194.1	1346.0	1501.2	1594.3	1688.0
I_G/I_{D1}=0.491	FWHM /cm^{-1}	162.88	164.0	146.6	89.2	101.7

[1]Raman shift; [2]Full width at half maximum.

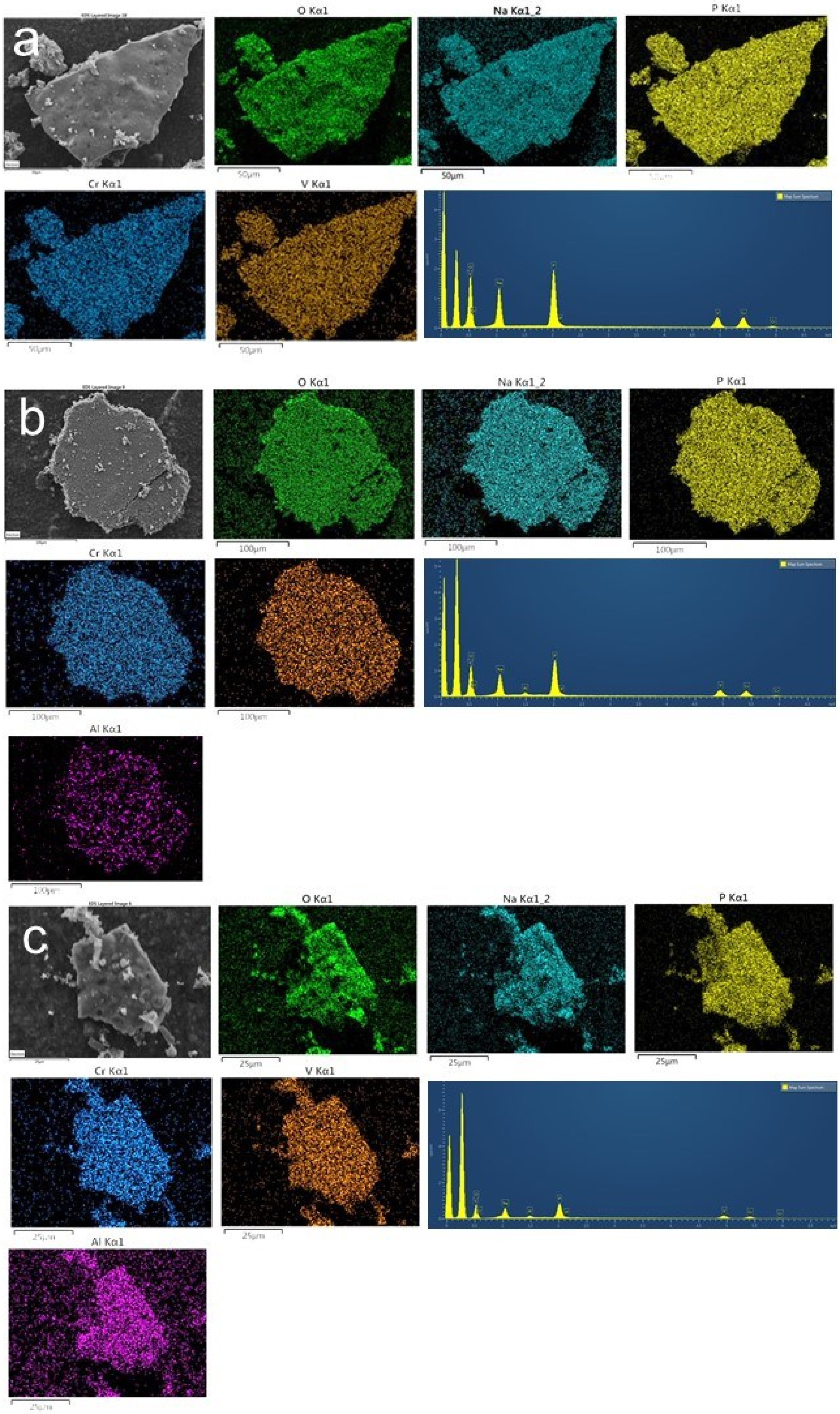

a
O Kα1
Na Kα1_2
P Kα1
Cr Kα1
V Kα1
50μm
b
O Kα1
Na Kα1_2
P Kα1
Cr Kα1
Al Kα1
100μm
c
O Kα1
Na Kα1_2
P Kα1
Cr Kα1
V Kα1
Al Kα1
25μm

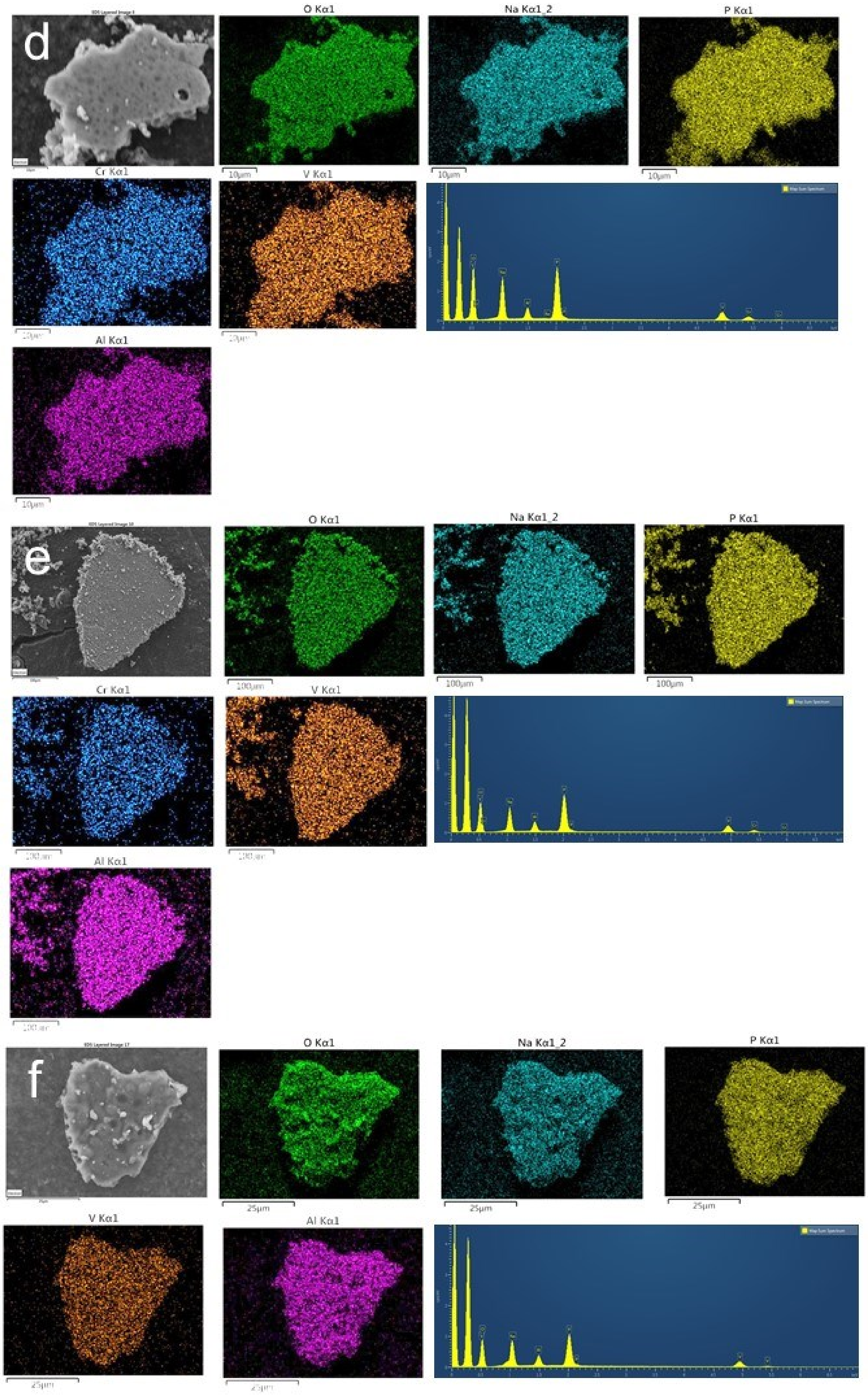

Figure S1. EDX spectra and maps for elements Na, V, Cr, Al, P, O recorded for raw samples with a) x= 0.0; b) x= 0.2; c) x= 0.4, d) x= 0.6, e) x= 0.8 and f) x= 1.0.

Table S2. Nominal and actual stoichiometry determined by EDX.

Nominal stoichiometry	Actual stoichiometry from EDX
$Na_3VCr(PO_4)_3$	$Na_{3.16}V_{0.86}Cr_{0.87}(P_{0.96}O_{4.08})_3$
$Na_3VAl_{0.2}Cr_{0.8}(PO_4)_3$	$Na_{2.80}V_{0.89}Al_{0.19}Cr_{0.74}(P_{0.98}O_{4.14})_3$
$Na_3VAl_{0.4}Cr_{0.6}(PO_4)_3$	$Na_{2.80}V_{0.96}Al_{0.38}Cr_{0.6}(P_{0.94}O_{4.14})_3$
$Na_3VAl_{0.6}Cr_{0.4}(PO_4)_3$	$Na_{3.28}V_{0.8}Al_{0.64}Cr_{0.32}(P_{0.94}O_{4.04})_3$
$Na_3VAl_{0.8}Cr_{0.2}(PO_4)_3$	$Na_{2.87}V_{0.91}Al_{0.76}Cr_{0.2}(P_{0.96}O_{4.12})_3$
$Na_3VAl(PO_4)_3$	$Na_{3.05}V_{0.85}Al_{0.93}(P_{0.97}O_{4.09})_3$

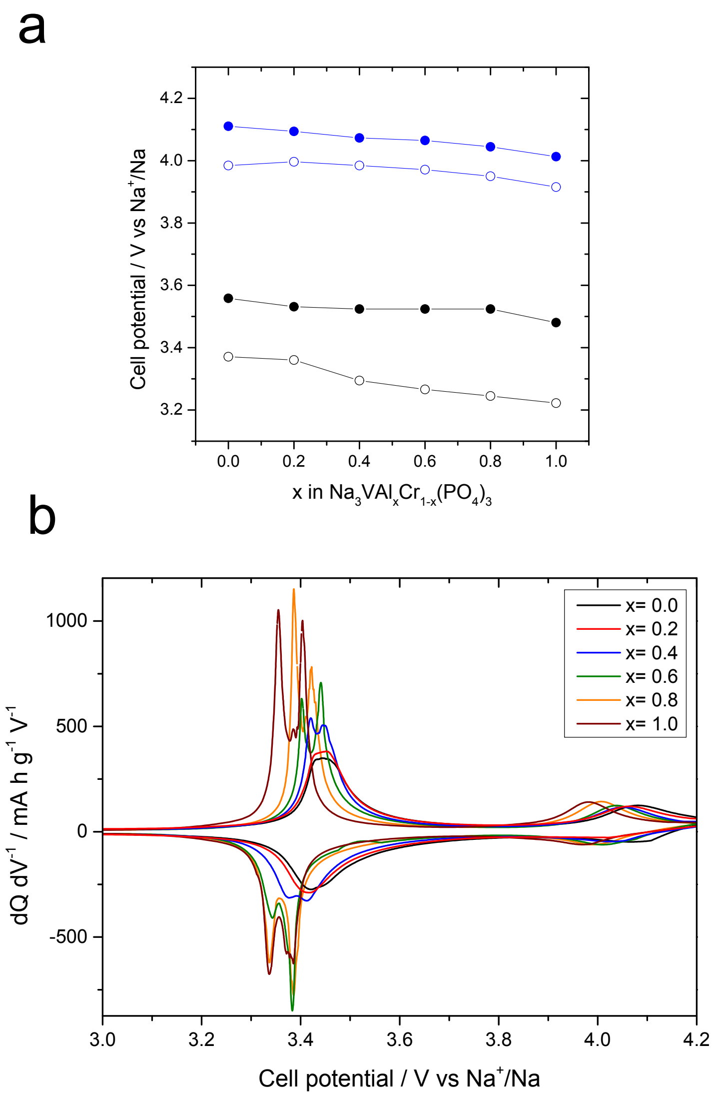

Figure S2. a) Plot of cell potential versus x in $Na_3VCr_{1-x}Al_x(PO_4)_3$; b) Differential capacity plots of the galvanostatic charge and discharge curves for $Na_3VCr_{1-x}Al_x(PO_4)_3$ ($0 \leq x \leq 1$) samples, recorded at C/10.

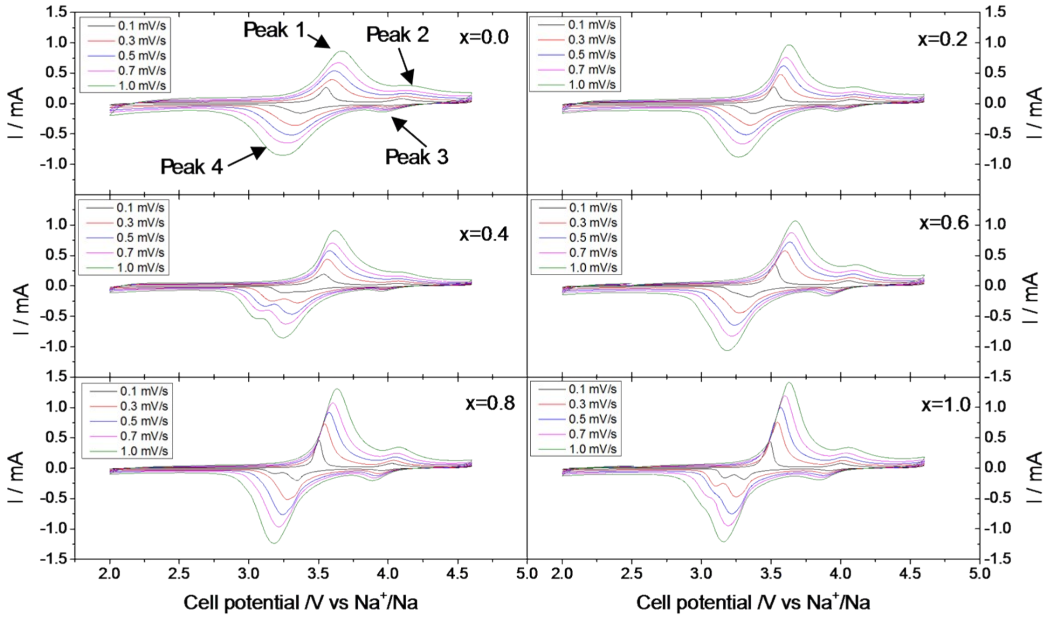

Figure S3. Cyclic voltammograms recorded for $Na_3VCr_{1-x}Al_x(PO_4)_3$ samples at several scan rates from 0.1 to 1 mV s^{-1} within the potential window of 2-4.6 V *vs* Na^+/Na. Peaks used for the calculation of diffusion coefficients have been labelled.

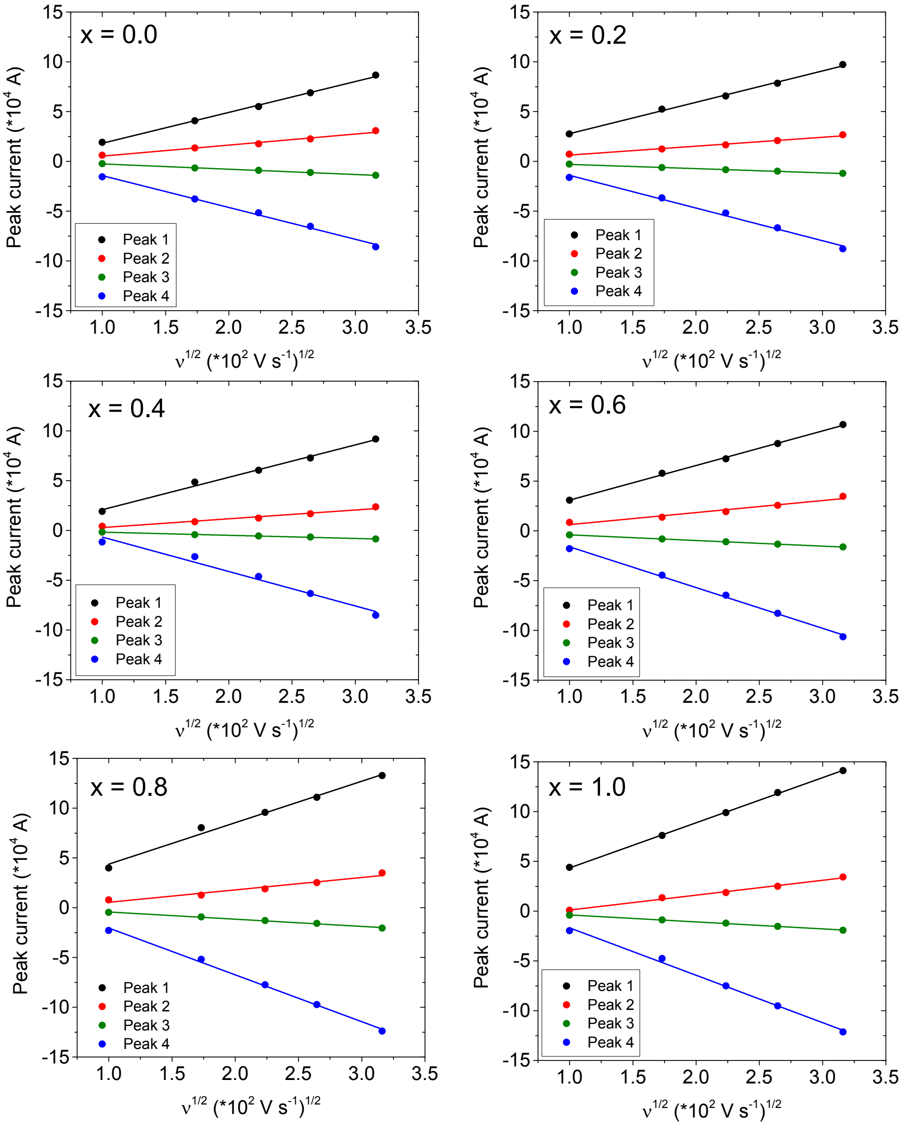

Figure S4. Linear plots liner relationship of the peak current (I_p) versus the square root of the scan rate ($\nu^{1/2}$) of $Na_3VCr_{1-x}Al_x(PO_4)_3$ (x= 0.0, 0.2, 0.4, 0.6, 0.8, 1.0) samples with the peaks current against the square root of scan rate.

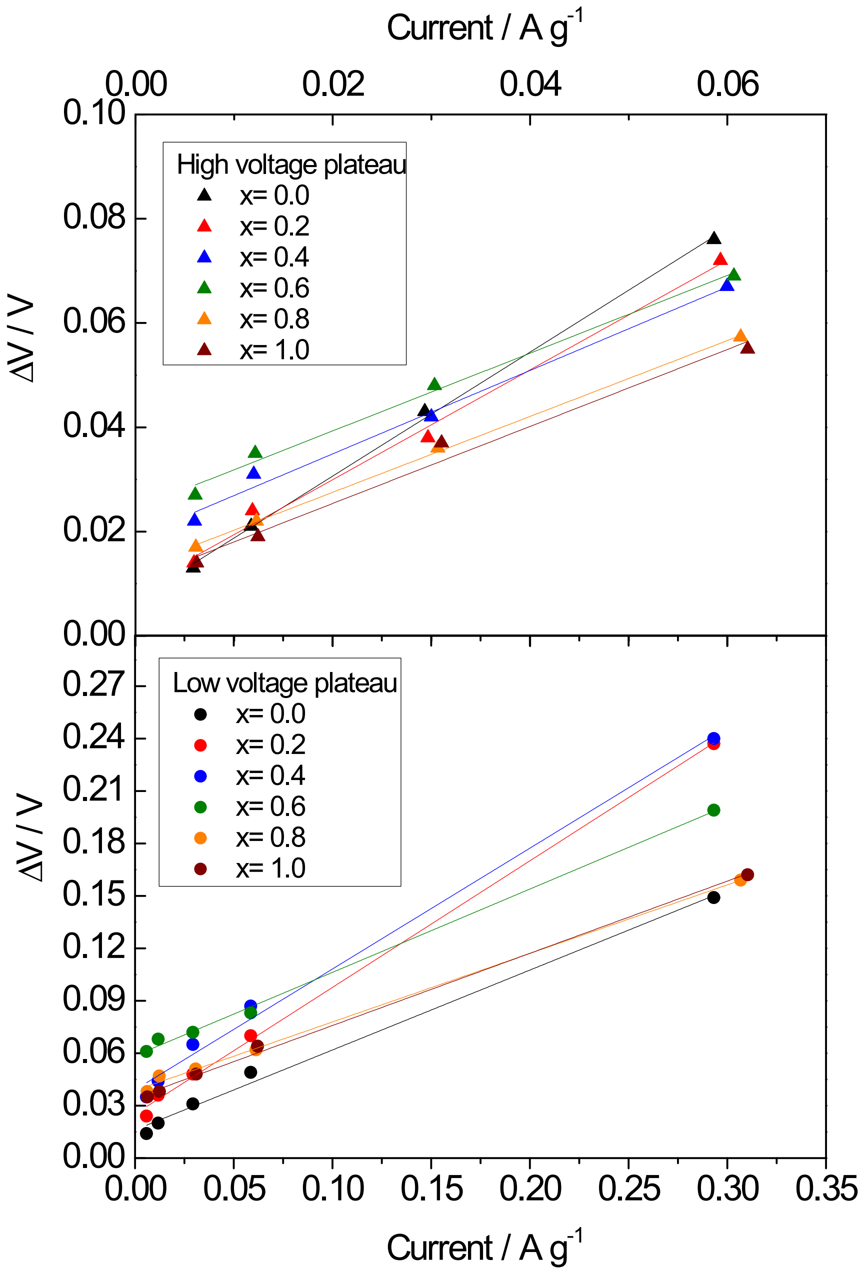

Figure S5. Plots of charge-discharge cell hysteresis (ΔV) versus applied current determined for both high and low voltage plateaus in the studied samples.

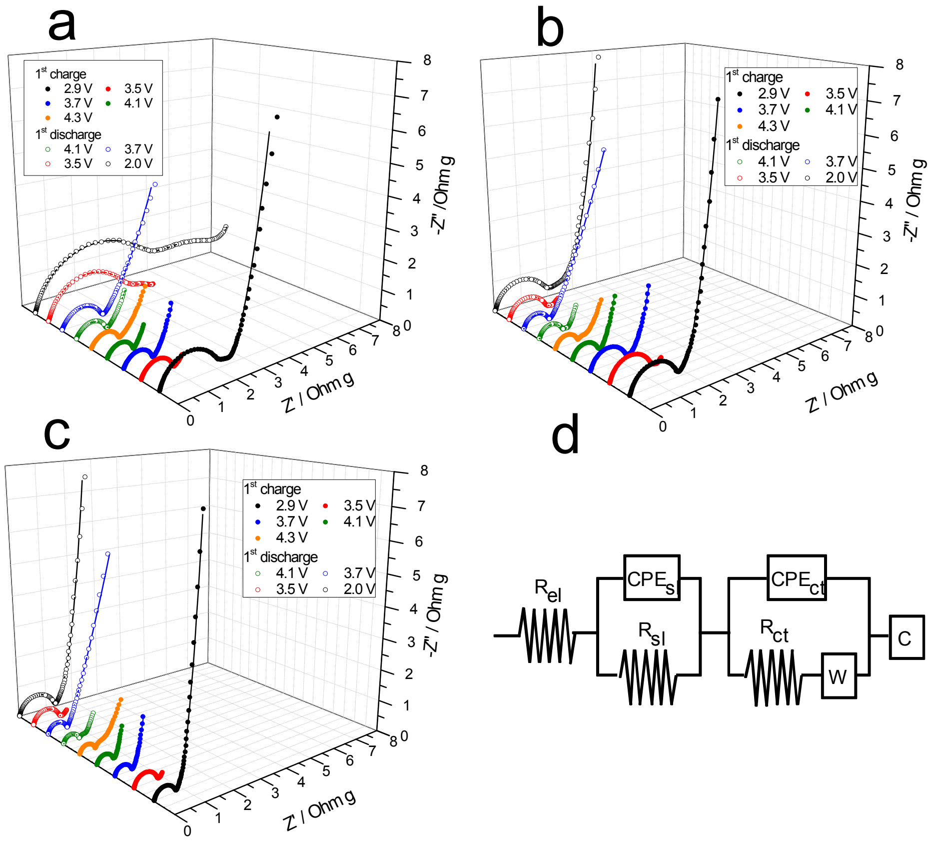

Figure S6. Experimental and fitted Nyquist plots of $Na_3VCr_{1-x}Al_x(PO_4)_3$ recorded for $Na_3VCr_{1-x}Al_x(PO_4)_3$ samples with x= a) x= 0.0, b) x= 0.2 and c) x= 1.0 at different depths of charge and discharge at a C/10; d) Equivalent circuit used for the fitting of the spectra.

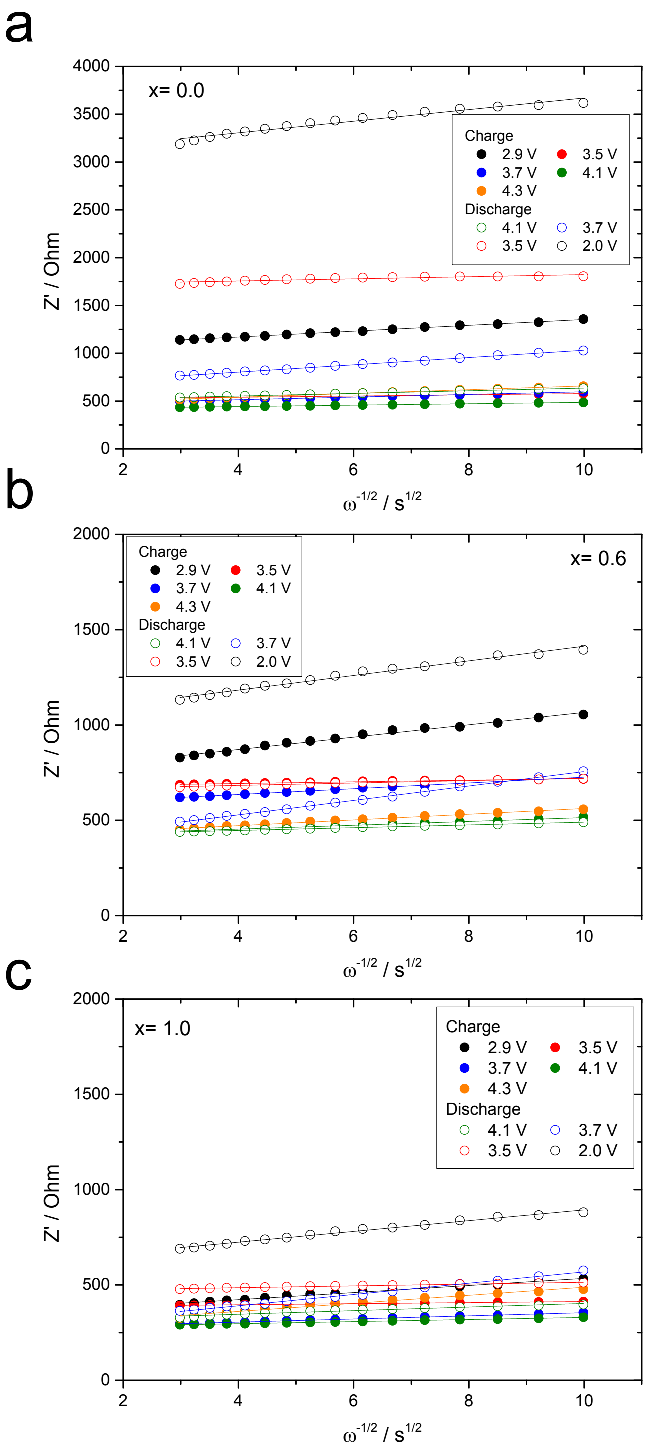

Figure S7. Linear plots of the real impedance versus the reciprocal square root of frequency, employed for the calculation of apparent diffusion coefficients of $Na_3VCr_{1-x}Al_x(PO_4)_3$ samples with x= a) 0.0, b) 0.2 and c) 1.0 at different depths of charge and discharge.